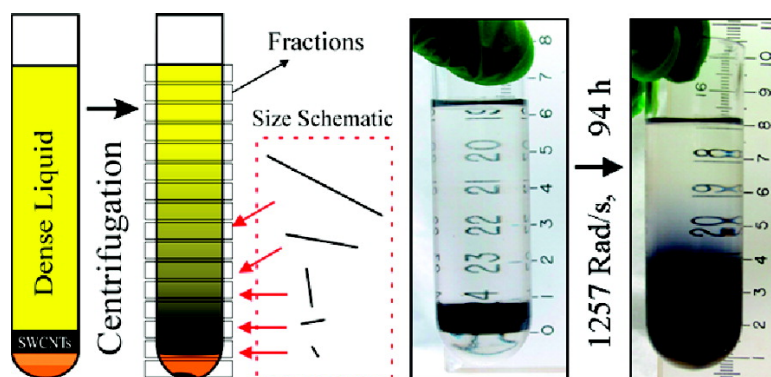


Centrifugal Length Separation of Carbon Nanotubes

Jeffrey A. Fagan, Matthew L. Becker, Jaehun Chun, Pingting Nie, Barry J. Bauer, Jeffrey R. Simpson, Angela Hight-Walker, and Erik K. Hobbie

Langmuir, 2008, 24 (24), 13880-13889 • Publication Date (Web): 20 November 2008

Downloaded from <http://pubs.acs.org> on December 10, 2008



More About This Article

Additional resources and features associated with this article are available within the HTML version:

- Supporting Information
- Access to high resolution figures
- Links to articles and content related to this article
- Copyright permission to reproduce figures and/or text from this article

[View the Full Text HTML](#)



Centrifugal Length Separation of Carbon Nanotubes

Jeffrey A. Fagan,^{*,†} Matthew L. Becker,[†] Jaehun Chun,^{†,§} Pingting Nie,[†] Barry J. Bauer,[†]
Jeffrey R. Simpson,^{‡,||} Angela Hight-Walker,[‡] and Erik K. Hobbie

Polymers Division and Physics Laboratory, National Institute of Standards and Technology,
Gaithersburg, Maryland 20899

Received May 5, 2008. Revised Manuscript Received October 1, 2008

Separation of single-wall carbon nanotubes (SWCNTs) by length via centrifugation in a high density medium, and the characterization of both the separated fractions and the centrifugation process are presented. Significant quantities of the separated SWCNTs ranging in average length from <50 nm to ~2 μm were produced, with the distribution width being coupled to the rate of the separation. Less rapid separation is shown to produce narrower distributions; these length fractions, produced using sodium deoxycholate dispersed SWCNTs, were characterized by UV–visible–near-infrared absorption and fluorescence spectroscopy, dynamic light scattering, Raman scattering, and atomic force microscopy. Several parameters of the separation were additionally explored: SWCNT concentration, added salt concentration, liquid density, rotor speed, surfactant concentration, and the processing temperature. The centrifugation technique is shown to support 10 mg per day scale processing and is applicable to all of the major SWCNT production methods. The cost per unit of the centrifugation-based separation is also demonstrated to be significantly less than size exclusion chromatography-based separations.

Introduction

The economical separation of single-wall carbon nanotubes (SWCNTs) by length and wrapping vector is an area of substantial ongoing research.^{1–14} Increasingly, efforts at separation are (rightfully) incorporated with purification efforts,¹⁵ for the removal of non-SWCNT carbon and metallic residues, and the individualization of the nanotubes via surfactant dispersion. Surfactant dispersion, whether using small molecule surfactants such as sodium dodecyl sulfate (SDS),¹⁶ sodium dodecyl-benzyl sulfate (NaDDBS),¹⁷ biological molecules such as DNA,³ or

bile salts^{6,18,19} such as either sodium cholate (NaChol) or sodium deoxycholate (DOC) typically involves two steps: sonication of the SWCNTs in the presence of the surfactant, and centrifugation to remove the less buoyant material, including much of the catalyst and amorphous carbon impurities. Starting from bile salt or DNA well-dispersed SWCNTs, both length and diameter separations can be achieved through additional centrifugation steps; in this contribution, the separation of DOC-dispersed SWCNTs is presented.

Since Svedberg^{20,21} developed high-speed and ultracentrifugation^{22,23} in the early 20th century, the separation of solutes with weak buoyancy differences has been feasible as a result of the enormous centripetal acceleration generated by such instruments. The primary concept of this work is to exploit the transient motion of the SWCNTs in response to an applied centripetal acceleration field to achieve length separation.²³ For rods of different aspect ratio but having the same diameter, the velocity of the rod scales approximately with the natural logarithm of the aspect ratio,²⁴ which allows for sufficient separation in a properly designed experiment to allow for fractionation.^{1,14} Arnold et al.^{5,6} additionally have recently demonstrated the use of ultracentrifugation to produce chirality separation of different diameter nanotubes by driving the position of the SWCNTs to their different isopycnic (equilibrium buoyancy) locations within a density gradient; a variation of this equilibrium technique^{12,13} allows for metal versus semiconducting SWCNT separation. The primary difference between the length and diameter separations is the relative size of the density difference between the different types of SWCNTs and the surrounding medium. In type separations, the density of the medium is set near the average density of the

* Corresponding author. E-mail: Jeffrey.fagan@NIST.gov.

† Polymers Division.

‡ Physics Laboratory.

§ Present address: Pacific Northwest National Laboratory, Richland, WA.

|| Present address: Physics Dept., Towson University, Towson, MD.

(1) Fagan, J. A.; Becker, M. L.; Chun, J.; Hobbie, E. K. *Adv. Mater.* **2008**, *20*, 1609–1613.

(2) Huang, X. Y.; McLean, R. S.; Zheng, M. *Anal. Chem.* **2005**, *77*, 6225.

(3) Zheng, M.; Jagota, A.; Semke, E. D.; Diner, B. A.; McLean, R. S.; Lustig, S. R.; Richardson, R. E.; Tassi, N. G. *Nat. Mater.* **2003**, *2*, 338.

(4) Fagan, J. A.; Simpson, J. R.; Bauer, B. J.; Lacerda, S.; Becker, M. L.; Chun, J.; Migler, K. B.; Hight Walker, A. R.; Hobbie, E. K. *J. Am. Chem. Soc.* **2007**, *129*(34), 10607–10612.

(5) Arnold, M. S.; Stupp, S. I.; Hersam, M. C. *Nano Lett.* **2005**, *5*, 713.

(6) Arnold, M. S.; Green, A. A.; Hulvat, J. F.; Stupp, S. I.; Hersam, M. C. *Nature Nanotech.* **2006**, *1*, 60–65.

(7) Heller, D. A.; Mayrhofer, R. M.; Baik, S.; Grinkova, Y. V.; Usrey, M. L.; Strano, M. S. *J. Am. Chem. Soc.* **2004**, *126*, 14567.

(8) Bauer, B. J.; Hobbie, E. K.; Becker, M. L. *Macromolecules* **2006**, *39*, 2637.

(9) Krupke, R.; Hennrich, F.; Kappes, M. M.; v. Löhneysen, H. *Nano Lett.* **2004**, *4*, 1395–1399.

(10) Chun, J.; Fagan, J. A.; Hobbie, E. K.; Bauer, B. *J. Anal. Chem.* **2008**, *80*(7), 2514–2523.

(11) Wei, L.; Wang, B.; Goh, T. H.; Li, L.; Yang, Y.; Chan-Park, M. B.; Chen, Y. *J. Phys. Chem. B* **2008**, *112*, 2771–2774.

(12) Yanagi, K.; Miyata, Y.; Kataura, H. *Appl. Phys. Express* **2008**, *1*, 034003.

(13) Green, A. A.; Hersam, M. C. *Nano Lett.* **2008**, *8*(5), 1417–1422.

(14) Nair, N.; Kim, W.; Braatz, R. D.; Strano, M. S. *Langmuir* **2008**, *24*(5), 1790–1795.

(15) Yu, A.; Bekyarova, E.; Itkis, M. E.; Fakhruddin, D.; Webster, R.; Haddon, R. C. *J. Am. Chem. Soc.* **2006**, *128*, 9902–9908.

(16) Bachtlo, S. M.; Strano, M. S.; Kittrell, C.; Hauge, R. H.; Smalley, R. E.; Weisman, R. B. *Science* **2002**, *298*, 2361.

(17) Islam, M. F.; Rojas, E.; Bergey, D. M.; Johnson, A. T.; Yodh, A. G. *Nano Lett.* **2003**, *3*, 269.

(18) Wenseleers, W.; Vlasov, I. I.; Goovaerts, E.; Obratsova, E.; Lobach, A. S.; Bouwen, A. *Adv. Funct. Mater.* **2004**, *14*, 1105–1112.

(19) Haggemueller, R., et al. *Langmuir* **2008**, *24*, 5070–5078.

(20) Svedberg, T.; Rinde, H. *J. Am. Chem. Soc.* **1924**, *46*, 2677–2693.

(21) Svedberg, T.; Pedersen, K. O. *The Ultracentrifuge*; Oxford University Press: London, England, 1940.

(22) Williams, J. W. *Ultracentrifugal Analysis in Theory and Experiment*; Academic Press: New York, 1962.

(23) Mächtle, W.; Börger, L. *Analytical Ultracentrifugation of Polymers and Nanoparticles*; Springer: Berlin-Heidelberg, Germany, 2006.

(24) Batchelor, G. K. *J. Fluid Mech.* **1970**, *44*, 419–440.

nanotubes to maximize the differences in density between SWCNT types; in length separation, the effect of the differences in density of various SWCNTs types is minimized by using a medium of much higher or lower density than the SWCNTs. We note that none of these techniques are exclusive of the others; serial separation can be performed to generate length and electronic type-sorted fractions. Chirality separation in a rate-based manner is also possible, but is not a focus of this contribution.

Theory

For individually dispersed SWCNTs, differences in the scaling of the buoyancy and frictional forces allows for length separation of the nanotubes via a rate separation scheme. A Nernst–Planck formulation can be used to model the flux, N_i , of each species i .

$$N_i = \frac{c_i F_{\text{buoyancy}}}{f_i} - D_i \nabla c_i + U c_i \quad (1)$$

Here, c_i is the concentration, f_i is the friction factor, and $D_i = k_B T / f_i$ is the diffusion coefficient of species i ; k_B is Boltzmann's constant, T is the temperature, and $k_B T$ is the thermal energy of the solution. U is the velocity of bulk fluid convection, which is expected to be zero in the absence of instrumental artifacts such as vibration or thermal gradient-driven mixing. The buoyant force, F_{buoyancy} , is

$$F_{\text{buoyancy}} = \pi r^2 l \times (\rho_s - \rho_{\text{SWCNT},i}) \times G \quad (2)$$

in which r is the radius of the SWCNT plus the surfactant shell, l is the tube length, ρ_s and $\rho_{\text{SWCNT},i}$ are the densities of the solution and the SWCNT (plus its surfactant shell), respectively, and G is the centripetal acceleration. Given the average parameters for the separations shown in this contribution, $|c_i F_{\text{buoyancy}} / f_i| \gg |D_i \nabla c_i|$, and the diffusive flux can be eliminated from eq 1. The dependence of the friction factor suggests the possibility of length-based separation. In the creeping flow limit, as indicated by a Reynolds number, $\text{Re} = V_i \rho_s l / \eta \ll 0.1$, in which $V_i(l) = F_{\text{buoyancy}} / f_i$ is the ballistic velocity of an individual SWCNT, the friction factor for a long, thin rod can be represented as²⁴

$$f_{\parallel} = \frac{2\pi\eta l}{\gamma} \left(\frac{1 + 0.307/\gamma}{1 - 0.5/\gamma} + 0.426/\gamma^2 \right),$$

$$f_{\perp} = \frac{4\pi\eta l}{\gamma} \left(\frac{1 + 0.307/\gamma}{1 + 0.5/\gamma} + 0.119/\gamma^2 \right) \quad (3)$$

where η is the fluid viscosity, and $\gamma = \ln(l/r)$. The effects of the separation rate, which affect the Reynolds number, are experimentally probed, and the results are presented in a later section of this paper; the maximum achieved Reynolds number was on the order of 10^{-6} . Combining eqs 1–3 yields an equation for the flux in which the nonlinear dependence on SWCNT length, approximately proportional to $\ln(l/r)$, is clearly apparent.

$N_i(l) \approx$

$$c_i \frac{(\rho_s - \rho_{\text{SWCNT},i}) G r^2}{6\eta} \frac{2\gamma^4 + 0.614\gamma^3 + 0.544\gamma^2 - 0.136}{\gamma^3 + 0.614\gamma^2 + 0.638\gamma + 0.0135} \quad (4)$$

Unlike many other materials, the radius of a SWCNT does not vary with its length; thus the consequence of the $\ln(l/r)$ dependence in eq 4 is that longer SWCNTs travel with a greater velocity in opposition to the applied acceleration.

Length separation, with minimal chirality differentiation, thus should occur in an experiment when $\Delta\rho = \rho_s - \langle\rho_{\text{SWCNT}}\rangle \gg \Delta\rho_{\text{SWCNT}}$

$= \langle\rho_{\text{SWCNT}}\rangle - \rho_{\text{SWCNT},i}$, where $\rho_{\text{SWCNT},i}$ is the density of an individual SWCNT chirality, and $\langle\rho_{\text{SWCNT}}\rangle$ is the average density of all the SWCNT types in solution. Alternatively, chirality separation should be maximized when $\Delta\rho \approx 0$ and different SWCNT types experience buoyancy forces in opposite directions.

Experimental²⁵

Cobalt–molybdenum catalyst method (CoMoCat)²⁶ (S-P95-02 grade, Batch NI6-A001, Southwest Nanotechnologies), SG grade CoMoCat (SG-000-0002, Southwest Nanotechnologies), high-pressure carbon monoxide decomposition (HiPco) (Batch 286, Carbon Nanotechnologies, Inc.), and laser ablation (NASA-JSC soot #338 and NanoPower Research Laboratories soot # NPRL-299) SWCNTs were dispersed in aqueous solution using 2% by mass DOC surfactant (Sigma). SWCNT prep consisted of sonication (tip sonicator, 0.64 cm, Thomas Scientific) of the SWCNT powder loaded at (1.0 ± 0.1) mg/mL in the 2% surfactant solution for 1.5 h in ~32 mL batches immersed in an ice water bath and tightly covered at ~30 W of applied power. Postsonication, each suspension was centrifuged at 21 000g in 1.5 mL centrifuge tubes for 2 h, or 35 000g for 2 h in 13 mL centrifuge tubes, and the supernatant was collected; the resulting rich black liquid contained primarily individually dispersed SWCNTs.

Density-modified solutions were generated by mixing the appropriate surfactant or SWCNT solution with iodixanol, (5,5'-(2-hydroxy-1-3-propanediyl)-bis(acetylamino)]-bis-[N,N'-bis(2,3-dihydroxypropyl)-2,4,6-triiodo-1,3-benzenecarboxamide]), purchased as Opti-Prep (Sigma)⁵ and 2% by mass DOC solution; all percentages listed for iodixanol solutions are for percent mass. Appropriate dilutions were additionally made where specified. For the experiments, the densities of the layers were chosen such that $\Delta\rho \gg \Delta\rho_{\text{SWCNT}}$ in the starting layer and for 5 cm above; a dense underlayer was also included. These liquid layers were performed by careful layering in either 17 or 38.5 mL centrifuge tubes (Beckman-Coulter #344061, #355631, respectively), with the center of the SWCNT layer defined as $z = 0$.

A Beckman-Coulter L80-XP ultracentrifuge with a swinging bucket SW.32 Ti rotor was used with either the SW-32 or the SW-32.1 bucket sets, depending on the experiment, for the length separation and postfractionation concentration of like fractions;²⁵ a VTi.50 vertical rotor was additionally used for concentration of some fractions. In length separation experiments, the total volume separated was scaled with the inner diameter of the chosen centrifuge tube, such that, for either SW-32 (38 mL) or SW-32.1 (17 mL) buckets, equivalent separation and fractions based on the distance traveled were achieved and collected. A common set of acceleration and deceleration settings for the rotor (Ramp setting 5, Decel. setting 5) were used in all runs, corresponding to gentle acceleration/deceleration to 183 rad/s over 4 min, followed/preceded by rapid acceleration/deceleration. In the larger buckets, the typical preparation contained 24 mL of liquid in four layers: 1 mL of 40% iodixanol, 1 mL of 30% iodixanol, 2 mL of 20% iodixanol containing the SWCNTs, and 20 mL of 18% iodixanol in the top layer. All layers contained 2% DOC. At the most common separation conditions, (1257 and 3142) rad/s, the maximum centripetal acceleration in the SW-32 rotor was, respectively, ~24600 and 153 700 times the acceleration due to gravity. For an 18% iodixanol layer $\Delta\rho \approx 45$ kg/m³, and $\Delta\rho_{\text{SWCNT}}$ is ~1.25 kg/m³ or less. After the separation, 16 (1.5 mL) individual fractions were collected in each case by hand pipetting from the top in 0.75 mL increments.

Concentration of like fractions was typically performed by the uniform filling of the appropriate centrifuge tube with the length-separated SWCNT solution, followed by ultracentrifugation. Under

(25) Certain equipment, instruments, or materials are identified in this paper in order to adequately specify the experimental details. Such identification does not imply recommendation by the National Institute of Standards and Technology nor does it imply the materials are necessarily the best available for the purpose.

(26) Kitiyanan, B.; Alvarez, W. E.; Harwell, J. H.; Resasco, D. E. *Chem. Phys. Lett.* **2003**, *317*, 497–503.

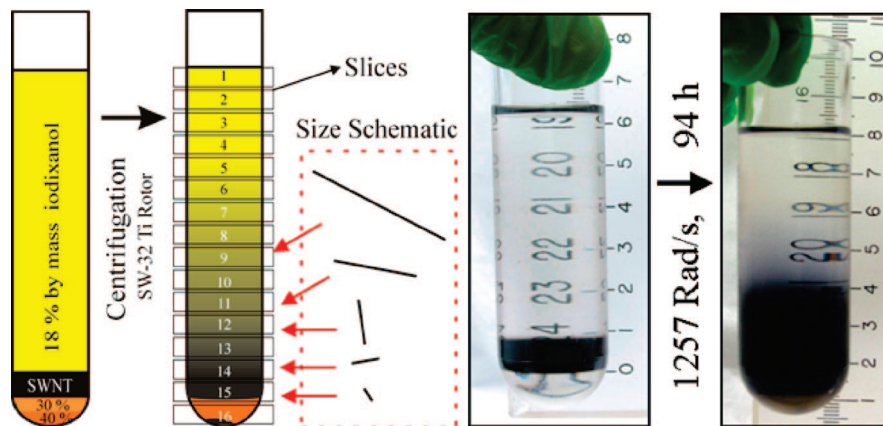


Figure 1. Schematic and photographs of the length separation by centrifugation process for CoMoCat SWCNTs at 1257 rad/s in DOC/iodixanol solution at 15 °C. An injection layer containing the SWCNTs, modified to the appropriate liquid density, is placed near the bottom of the tube to maximize the separation. Longer nanotubes move farther in response to the applied centrifugation, and thus separate up the tube; any high density impurities move in the opposite direction.

these conditions, the sedimentation of the iodixanol gradually causes the SWCNTs to be excluded from both the bottom (as the iodixanol is more dense) and the top (as the SWCNTs are more dense than the surfactant alone) of the tube. Dilution of the top one-half to two-thirds of the individual length fraction with additional stock surfactant solution, to lower the average density in the top part of the tube, dramatically speeds this process. Some of these concentrated fractions were then additionally processed by dialysis against 0.8% DOC solution in 25 kD molecular weight cut-off (MWCO) dialysis floats to remove the remaining iodixanol and to reduce the total surfactant concentration.

Ultraviolet–visible–near-infrared (UV–vis–NIR) absorbance spectroscopy was performed in transmission mode on a PerkinElmer Lambda 950 UV–vis–NIR spectrophotometer over the range of 2500–185 nm for SWCNT–surfactant solutions, and from 1450–325 nm for SWCNT–surfactant–iodixanol solutions. Measurements were typically performed on the extracted fractions in a 2 mm path length quartz cuvette. In all cases, the incident light was circularly polarized prior to the sample compartment, and the spectra corrected for both dark current and background. Data was recorded at 1 nm increments with an instrument integration time of at least 0.12 s per increment. The reference beam was left unobstructed, and the subtraction of the appropriate reference sample was performed during data reduction.

Dynamic light scattering (DLS) was performed in a temperature controlled cell maintained at 25 °C using a Brookhaven Instruments BI-200SM in VH (crossed polarizers) configuration with 532 nm excitation. Scattering was measured at a minimum of three different angles with a minimum of two repetitions. Dialyzed samples were used for these measurements. The correlation of scattering intensity in each case was fit to a double exponential, and the resultant inverse rotational relaxation time is of the faster mode related to the squared magnitude of the scattering vector and the rotational diffusion coefficient in accordance with formalism of Pecora.²⁷ SWCNT length was obtained from D_r .²⁸

Tapping-mode atomic force microscopy (AFM) measurements were conducted in air using a Nanoscope IV system (Digital Instruments) operated under ambient conditions with 1–10 Ohm/cm, phosphorus (*n*) doped silicon tips (Veeco; RTESP5, 125 μm length; 30 μm width, normal spring constant, 40 N/m; resonance frequency, 240 kHz to 300 kHz). Length separated, concentrated and dialyzed fractions were diluted 10× in water (18 MΩ cm⁻¹) prior to being deposited (2 μL) onto freshly cleaved mica. After being allowed to dry, the entire sample was cleaned of surfactant with an ethyl acetate wash/wicking procedure to afford clear imaging

conditions. Lengths of nonoverlapping and identifiable SWCNTs were counted within the Nanoscope software.

Raman spectra were collected in a collinear backscattering configuration. An Ar+ laser (Coherent Innova Sabre with multiline visible head) provided the excitation; approximately 20 mW of power was focused to a spot size of approximately 100 μm within the sample volume. Samples were measured in a single semimicrospectrophotometer cell (NSG, 10 mm path length) that was held immobile for all of the measurements. The spontaneous Raman backscattered light was collected with a triple grating spectrometer (Dilor XY800) and a liquid nitrogen cooled CCD detector. The signal was integrated for an appropriate time to obtain a signal-to-noise ratio greater than 50. The integration time for the CoMoCat fractions shown here was 10 s averaged over four scans. Data were collected with excitation at 514.5 nm. At the 514.5 nm excitation line Raman frequency shifts in the range (150 to 4000) cm⁻¹ were measured, with specific attention given to those between (150 and 2800) cm⁻¹. Data were corrected solely by scaling for incident laser intensity and by the subtraction of a small background, generally less than a few percent of the feature intensity.

NIR fluorescence spectra were recorded using a Horiba Jobin Yvon nanolog-3 spectrofluorometer with a liquid N₂-cooled InGaAs detector. Emission spectra were corrected for the instrument's source spectral distribution and detector spectral response using intensity calibration data provided by the manufacturer, and for the absorbance of the filter used to restrict scattered excitation light from the NIR monochromators and detector. Excitation wavelength was scanned in 5 nm increments using a 450 W xenon lamp through an 8 nm slit and emission collected at 90° in 2 nm increments through an 8 nm slit. To account for differences in concentration, fractions were diluted to a common absorbance ≈ 0.05/cm at 775 nm, and were measured in a 10 mm square quartz cuvette.

Unless stated otherwise, the standard uncertainty throughout this contribution is denoted by error bars equal to one standard deviation.

Results and Discussion

A schematic and photograph of the experiment are shown in Figure 1. The band containing the SWCNTs is clearly visible. Measured lengths for the S-P95-02 CoMoCat SWCNTs shown in Figure 1 from the collected fractions are presented in Figure 2; spectra, scaled for concentrations at 775 nm are shown in Figure 4A. When run to optimize the transient motion of the SWCNTs, high resolution of the separated lengths is achievable, and spectra showing well-defined SWCNT peak features with increasing peak to baseline ratios are measured above the injection layer. SWCNT bundles, as determined by peak broadening, a red shift in peak location, and a decrease in peak absorption are

(27) Pecora, R. *Annu. Rev. Biophys. Bioeng.* **1972**, *1*, 257–276.

(28) Doi, M.; Edwards, S. F. *The Theory of Polymer Dynamics*; Clarendon Press: Oxford, England, 1986.

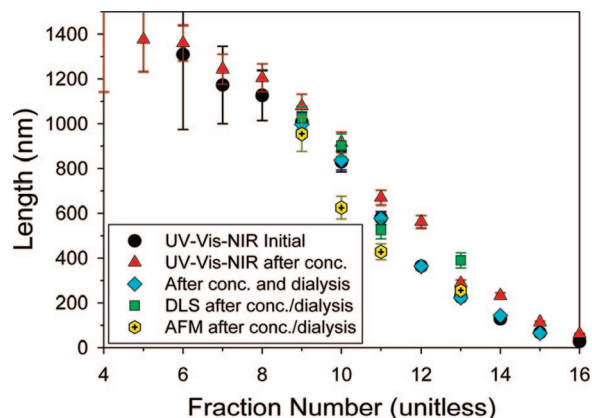


Figure 2. SWCNT length versus fraction number as measured by UV-vis-NIR, DLS and AFM. Values for the UV-vis-NIR projected the length for the initial fractions as extracted from the tube and after centrifugal concentration and then dialysis to remove the iodixanol, and as measured by AFM and DLS for fractions separated at 1257 rad/s. Concentration and dialysis, necessary for DLS and AFM, both appear to slightly modify the average length of the SWCNTs remaining in solution. The agreement of the UV-vis-NIR projections with the AFM and DLS values is reasonable; the differences may be explained by systematic difficulties in undercounting longer SWCNTs in AFM, as they tend to overlap other SWCNTs, and the length weighting of the UV-vis-NIR and DLS techniques. Error bars (1 std. deviation) are based on the instrument error and a 5% error in the slope of eq 5 for the UV-vis-NIR projections; error bars for AFM are the standard deviation of the mean calculated from 150 counted SWCNTs for each fraction.

typically not observed in centrifuged DOC solutions, but would be expected to fractionate downward; high density impurities are indeed seen to fractionate to the bottom of the tube and are not resuspended during fraction collection.

As previously detailed,^{1,4} the oscillator strength of the optical transitions can also be used to empirically calculate the (length weighted) average length of the separated fractions. In particular, an empirical relationship between the peak to baseline ratio and length was measured for the specific batch of S-P95-02 grade CoMoCat fractions used in this contribution in a publication in which size exclusion chromatography (SEC) was used to generate length separation;⁴ this relation is eq 5. The degree of SWCNT individualization has previously been shown to be similar and approximately complete in both DNA and DOC dispersion,¹⁹ so the same relation can be applied for this contribution. Further discussion of eq 5 is presented in the Supporting Information.

$$l(\text{nm}) \approx \left(\frac{\text{Absorbance}(984 \text{ nm})}{\text{Absorbance}(775 \text{ nm})} - 0.842 \right) \times 160.4 \text{ nm} \quad (5)$$

The length of the separated fractions was also separately determined using DLS and AFM. The values of the length from DLS, UV-vis-NIR, and AFM for the fractions generated by centrifugation at 1257 rad/s, shown in Figure 1, are shown in Figure 2; AFM images of selected fractions are presented in Figure 3.

DLS was performed in VH scattering mode, and the length is measured from the extrapolated intercept at zero scattering vector for the inverse rotational relaxation time, which is equal to 6 times the rotational diffusion coefficient,^{7,8}

$$D_r = 3k_B T \left(\frac{\ln(l/2r) - 0.8}{\pi \eta l^3} \right) \quad (6)$$

The measured scattering for the fractions shown in Figure 1 are plotted in the Supporting Information. The DLS experiment was repeated at a reduced ($\sim 1/3$) SWCNT concentration to look for

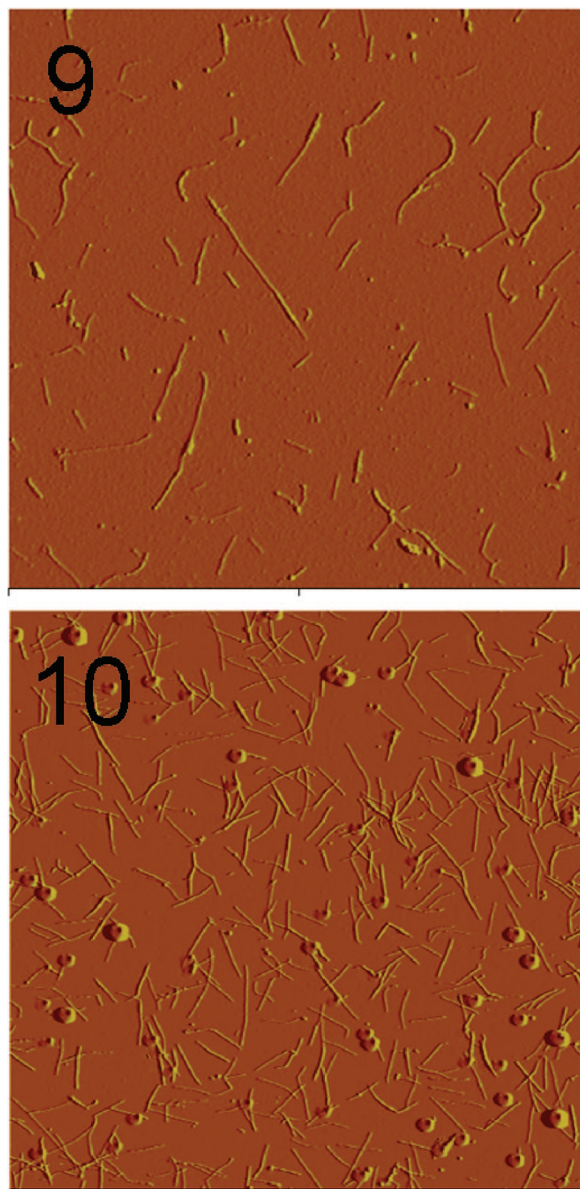


Figure 3. AFM images on mica of fractions 9 and 10 of the length-separated SWCNT fractions from the separation pictured in Figure 1. These fractions were concentrated, and then dialyzed to remove the remaining iodixanol and excess surfactant prior to deposition for imaging. The size of both images is $5 \mu\text{m}$ by $5 \mu\text{m}$. Small surfactant islands are visible in the image of fraction 10.

any SWCNT concentration effects. The SWCNTs were found to behave similarly at the reduced concentration, indicating that the SWCNT concentration does not strongly affect the effective size of the SWCNTs in the dispersion.

AFM values are based on contour lengths measured for approximately 150 SWCNTs for each fraction. Images of several of the 1257 rad/s separated SWCNT fractions shown in Figure 2 are presented in Figure 3. The typical variance in the average length is approximately 20% for each of the measured fractions. The values measured using AFM show reasonable agreement to the values obtained via eq 5 and from DLS; the differences may be explained by systematic difficulties in undercounting longer SWCNTs in AFM, as they tend to overlap other SWCNTs, and the length weighting of the UV-vis-NIR and DLS techniques. Specifically, the difficulty in depositing individualized SWCNTs for imaging in AFM may affect the observed average length if there is preferential attachment or rearrangement on the surface

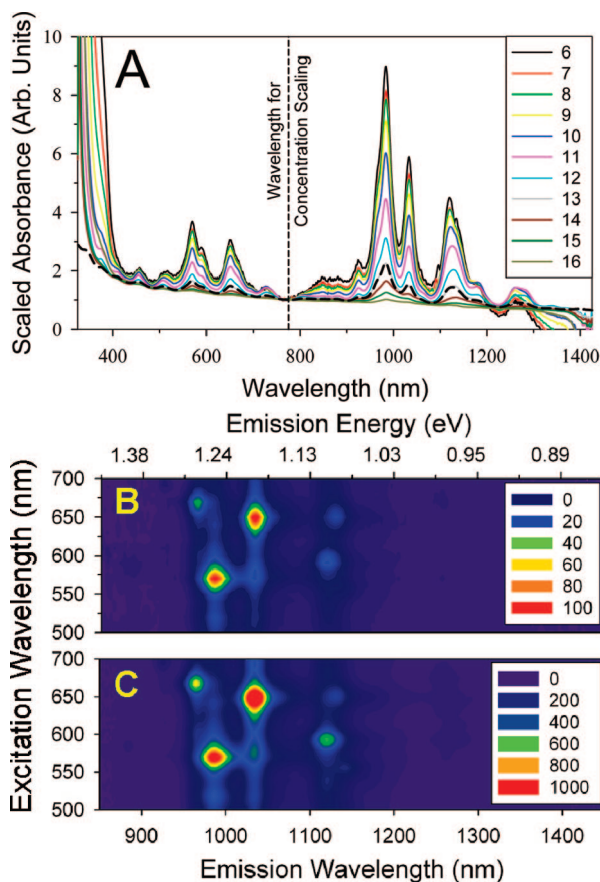


Figure 4. (A) Scaled absorbance spectra of the length sorted nanotube fractions shown in Figures 1 and 2. Below 400 nm and above 1200 nm, the curves are affected by the absorption of the density medium. The strength of the intrinsic SWCNT optical features increases strongly with the SWCNT length, whereas the relative sizes of the features to each other do not change significantly across the fractions. These results indicate length separation without chirality separation. The absorption spectrum for the SWCNT mixture prior to separation (dashed spectra) is also shown. (B,C) NIR fluorescence contour plots for the very dilute dispersions of unsorted SWCNTs (B), and fraction 6 from the 1257 rad/s separation shown in Figures 1 and 2 (C). The color scale bars indicate the real intensity increase in the fluorescence with the length separation; the fact that the relative intensities of the features is unchanged indicates that no preferential type separation is occurring.

with length, and from the increased likelihood that longer SWCNTs will overlap other SWCNTs in an image and thus not be counted.

The change in the strength of the optical transitions, but not in the type distribution of the SWCNTs is observable both in the UV-vis-NIR absorbance spectra and in the NIR fluorescence of the SWCNTs. Absorbance spectra, scaled by the value of the background-subtracted absorbance at 775 nm, are plotted in Figure 4A for the S-P95-02 grade CoMoCat fractions shown in Figure 1; the NIR fluorescence from E_{22} excitation of the unsorted CoMoCat SWCNTs and from fraction 6 of the separated material are shown in Figure 4B,C respectively. In both figures, it is clear that the relative distribution of the peaks changes insignificantly across the fractions, despite the large increase in the intensity of the features in the longer fractions.

Given the high resolution of the SWCNT fractions generated by the 1257 rad/s separation, as demonstrated in Figures 2 and 3, significant additional characterization of those fractions was performed. Dialysis of the separated fractions to remove the iodixanol allows for resonant Raman interrogation of the fractions without the presence of the richly featured iodixanol Raman

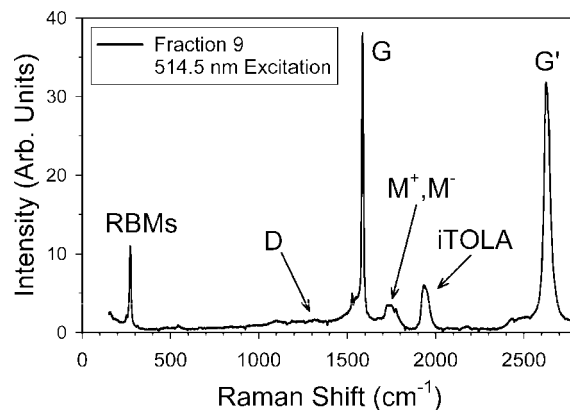


Figure 5. Raman scattering from fraction 9, after dialysis to remove the iodixanol, of the 1257 rad/s sorted CoMoCat fractions presented in Figures 1–6. The excitation wavelength was 514.5 nm. Strong features due to the RBMs, G, G' , iTOLA, M^+ , and M^- bands are clearly visible; the D band is measurable at 1328 cm^{-1} , but is insignificant on the scale of the figure. The G/D band ratio is $\sim 250:1$ for fraction 9. Because of partial excitation of the metallic-type SWCNTs in the CoMoCat sample some Breit–Wigner–Fano broadening of the G band is observed. The stochastic noise is less than the line thickness; a small background contribution, which did not affect the relative feature size, was subtracted.

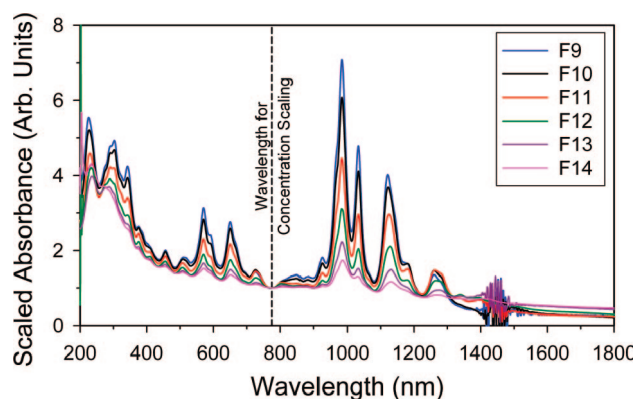


Figure 6. Scaled absorbance spectra of length sorted fractions 9, through 14 after concentration and dialysis to remove the iodixanol density media. The SWCNT optical transitions are clearly increased by the length separation, whereas the π -plasmon type absorption is much less sensitive to the SWCNT length. Multiple E_{11} (~ 800 – 1400 nm), E_{22} (~ 500 – 750 nm), E_{33} (~ 300 – 400 nm), and overlapped E_{44} (at ~ 250 – 300 nm) optical transitions are observed.

spectrum. In Figure 5, the resonant Raman features at 514.5 nm excitation are shown for fraction 9. Additional spectra, displaying the same features but with lower magnitudes, are provided in the Supporting Information for fractions 10, 11, and 13. Strong features due to the radial breathing modes (RBMs), G, G' , iTOLA, M^+ , and M^- bands are clearly visible; the D band is measurable at 1328 cm^{-1} , but is insignificant on the scale of the figure. At this wavelength, the G/D ratio is $\sim 250:1$ for fraction 9, and is ~ 170 , 92, and 47 for fractions 10, 11, and 13 respectively.

Dialysis of the separated fractions also allows for the interrogation of the absorbance in the UV spectrum. In Figure 6, the absorbance features attributable to the E_{33} excitation clearly become stronger and more distinct, as well as the E_{11} and E_{22} features, with the increase in the SWCNT length. The longer fractions are distinctly colored due to the large E_{22} features relative to the baseline absorbance in the visible region. Figure 7 is a picture of several fractions from different parent solutions showing the colored solutions that result from the length separations; the solutions labeled CoMoCat type 1 are fractions 6 and 8 from the

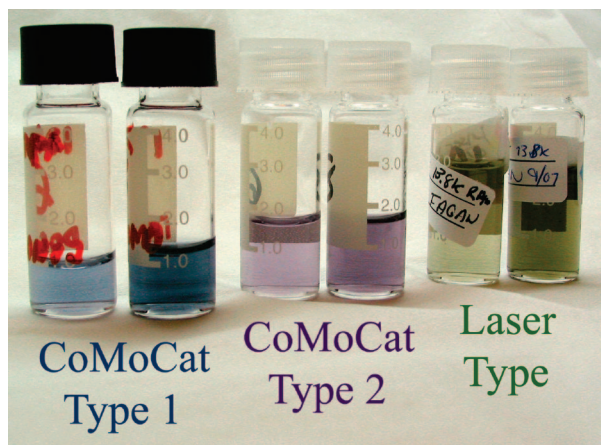


Figure 7. Photograph of the different color SWCNT solutions that result from length separation of different type distributions of SWCNT starting material. Fractions 6 and 8 are shown for 1257 rad/s separation of CoMoCat starting materials S-P95-02 and SG-000-0002 (left and center, respectively), and fractions 9 and 10 for 1445 rad/s separation of NASA-JSC soot #338 laser ablation type SWCNTs. Note that solely length and not chirality separation of the black parent solutions has occurred: the CoMoCat materials each contain roughly 15 contributing SWCNT types, and the Laser sample likely contains 30 or more.

S-P95-02 grade CoMoCat material separated at 1257 rad/s detailed earlier in this contribution. Chiral angle, or metal versus semiconducting separations would reveal that a combination of many individual colors contribute to the colors observed in Figure 7, as recent results of Green and Hersam¹³ and Yanagi et al.¹² demonstrate.

As in Figure 4, it can be seen in Figure 6 that the relative distribution of chiralities in the sample is not significantly altered by the length separation process. Chirality separation would appear as a dramatic shift in the relative intensity of the different transitions, shifting the relative sizes of the peaks roughly the same amount for each of the E_{11} , E_{22} , and E_{33} transitions. However, further processing to produce such chirality enriched samples is possible using either the isopycnic method or rate-based techniques.

Alternate scaling of the spectra in Figure 6 for carbon concentration, either by π -plasmon region absorbance or by the absorbance in the 1600–1800 nm region, does not significantly change the relative increase in the size of the absorption features with length. However, the exact shape of the absorbance below 220 nm as shown in Figure 6 may be affected by slight differences in the DOC content of the samples, which strongly absorbs in this region, with respect to the reference solution; the noise around 1450 nm in the spectra is due to inaccuracy in the subtraction of the strongly absorbing water feature at this wavelength.

Independent measurement of the SWCNT lengths in the various fractions by AFM and DLS, as detailed in Figure 2, demonstrates that the strength of the SWCNT optical transitions follow the empirical relation, eq 5, that we previously noted in DNA-wrapped SEC-sorted SWCNTs. A plot of the optical strength of the E_{11} transition for the (6,5) nanotube for both the SEC- and centrifugation-sorted SWCNTs is presented in the Supporting Information.

As demonstrated previously, and in the results shown above, SWCNTs can be separated by length through centrifugation in a dense medium. However, the degree and precision of the separation depend upon the chosen parameters for the separation. Several experimental variables are easily modifiable: separation rate, SWCNT concentration, the race layer density, and the bulk temperature of the solution.

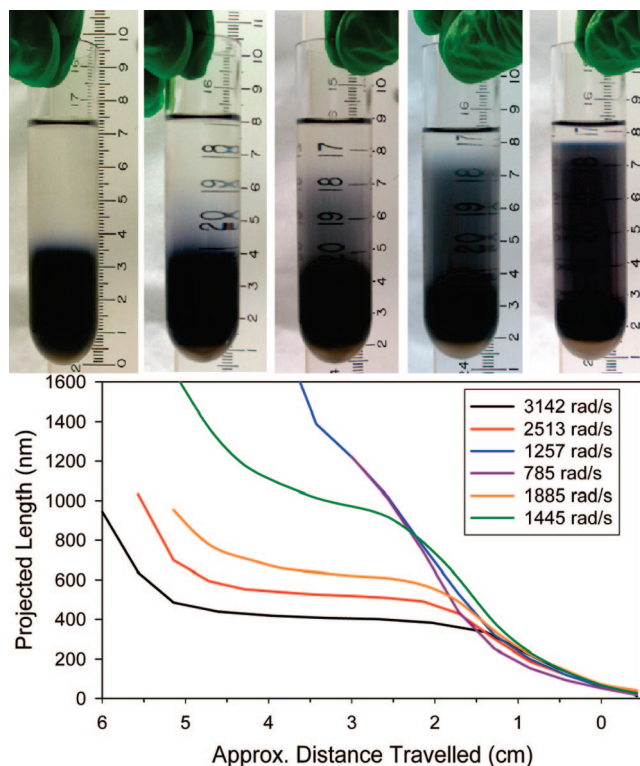


Figure 8. (A) Photographs, left to right, of SWCNTs separated at 785, 1257, 1570, 2513, and 3142 rad/s. Note that the furthest distance traveled by the SWCNTs increases with the separation rate, although the total integrated acceleration is constant across the experiments. The distribution of the separated SWCNTs within the race layer is also seen to change with the separation rate. Note that the aspect ratio of the images has been uniformly increased slightly to fit the images into the figure. (B) UV–vis–NIR projected lengths for the fractions from the different rates of separation. Although the SWCNTs travel the least in the 785 and 1257 rad/s, the separation achieved is closest to the theoretical expectation. The plateau region that develops at higher rates of separation is due to mixing of different length SWCNTs.

An increase in the rate of separation, i.e., an increase in the rotor RPM, but maintaining the total integrated acceleration, $\propto f\omega^2 dt$, generates surprising differences in the achieved separation. Figure 8A contains photographs of the separation at 785, 1257, 1570, 2513, and 3142 rad/s, while Figure 8B displays the UV–vis–NIR projected lengths for the separated fractions. Performing the separation at a higher rate under these conditions leads to the formation of a plateau feature in the average length curve, with the average length monotonically decreasing within this plateau feature with the increasing separation rate. To probe the cause of the change in the separation with rotation speed, several additional experiments were performed at 3142 rad/s. These included a preparation with approximately 20 mM of additional NaCl in each layer, and a preparation with less DOC surfactant (1%) in the layers. No significant change in the 3142 rad/s separation was identified in either of these experiments (data not shown).

Changes in the achieved separation were, however, also found to occur with an increase in the density of the liquid layers in the centrifuge tube. This is shown in Figure 9, in which five tubes are shown where the race layers were 14, 16, 18, 25, and 30% iodixanol, respectively, and the separation was performed at 1257 rad/s as in the experiment presented in Figures 1 and 2. Interestingly, the changes in the separation with the race layer density mimic the changes that occur as a result of an increased rotor speed, with the same turnover and plateau features observed in the apparent average length versus distance curves. Reducing

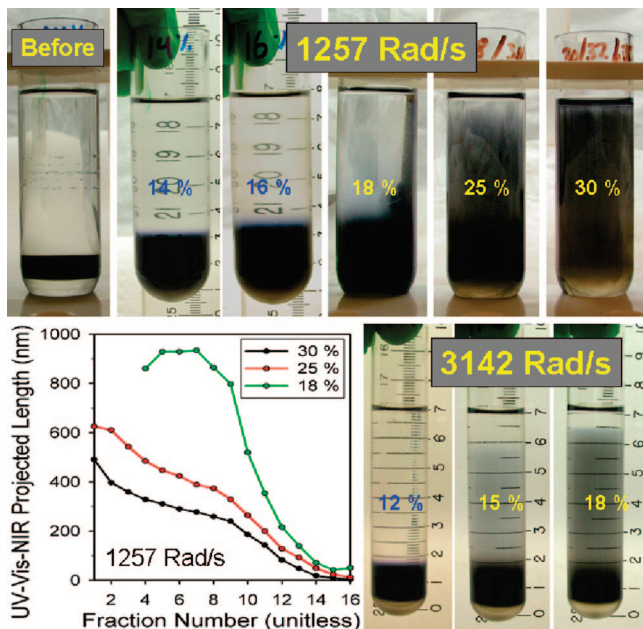


Figure 9. Photographs (top) and apparent SWCNT length versus distance traveled curves (bottom left) for the separation of CoMoCat SWCNTs at 1257 rad/s using different density race layers. Similar changes are shown in photographs for 3142 rad/s (bottom right). As expected, at 1257 rad/s, the distance traveled increases with the density of the race layer. However, the separation also becomes less ideal beyond a top layer composition of 18% iodixanol, similar to the effect measured due to an increase in the applied centripetal acceleration. For separation at 3142 rad/s the separation is more ideal at 15% than at 18%; however, at 12% iodixanol in the race layer, a mixture of chirality and length separation occurs.

the race layer density also changes the separation. This is shown for separation at 3142 rad/s in the bottom right of Figure 9. The reduction in layer density from 18% to 15% actually improves the separation, as can be seen in the projected length. However, with a top layer of 12% iodixanol, separation occurs due to both length and chirality, and the length cannot be projected from the absorbance due to this chirality redistribution. The top fraction of the concentrated band was found to be heavily enriched in the lower density (6,5) chirality.

Although each of the experiments shown in Figures 8 and Figures 9 contained an identical concentration of SWCNTs within the injection layer, for scaling up the separation process, the exact effects of SWCNT concentration on the measured separation could be highly important. Thus, separation experiments were performed with fractional SWCNT concentrations of 4.95 \times , 1.95 \times , 1/2, and 1/5 the typical inoculation. In absolute terms, 1 \times is a concentration \sim 0.24 mg/mL within the SWCNT layer in the centrifuge tube, as determined using an estimated extinction coefficient at 775 nm of 26000 cm²/g.²⁹ The results of the separation, performed at 3142 rad/s, are shown in Figure 10. Surprisingly, the average length of the SWCNTs within the plateau feature increases with additional SWCNT inoculation concentration, actually improving the effected separation.

The effect of the bulk temperature during the separation was also explored. Runs at 5 and 15 °C were equilibrated to temperature prior to the run within the ultracentrifuge. For the 40 °C separation, the rotor, rotor buckets, and solutions were equilibrated to the proper temperature by immersion in a thermostatic bath for several hours prior to introduction to the centrifuge chamber. The effects of the temperature on the

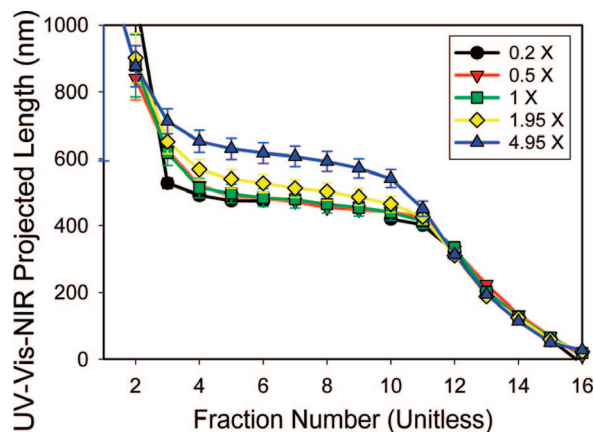


Figure 10. Effects of the initial SWCNT concentration on the average length of the SWCNTs extracted from the different layers after separation at 3142 rad/s for 15 h at 15 °C; 1 \times corresponds to a concentration of \sim 0.24 mg/mL within the centrifuge tube. No significant change is observed in the postseparation distribution of lengths with reduction in the initial concentration. A shift toward improved separation is noted with an increase in the SWCNT concentration, i.e., for higher mass throughput.

separation are shown in Figure 11. Surprisingly, the reduction in temperature, even from 15 to 5 °C, causes a significant redistribution of the SWCNT concentration in the solution. This redistribution, as with increasing concentration, also generally improves the separation as discussed below.

Plotting the fractional concentration profile versus fraction number for four of the different separation profile speeds shown in Figure 8 in Figure 12, it can be inferred that the plateau feature observed at higher separation rate is due to a mixture of different lengths in those fractions, and not due to a different spatial distribution of well-resolved lengths. This is visible in the dramatic reduction in the concentration of the short SWCNTs in the fraction approximately 0.5 cm from the injection layer with the increase in the separation rate from 1257 rad/s to 3142 rad/s. The plateau feature in the higher rate separations is the result of this short material being mixed upward in the liquid column, and reducing the average length of those fractions. A rate of 1257 rad/s generated the steepest projected length curve under these experimental conditions; including the information of the relative concentration for each average length, it is clear that this separation resulted in the greatest resolution of length in the different fractions. Integrating each of the concentration and length curves to calculate an average length value for the separated SWCNTs yields a value of 225 ± 5 nm in each case, equal to the average length projected by UV-vis-NIR absorbance for the unsorted material of \sim 220 nm.

A comparison of the measured average length versus distance traveled curves from the 1257 rad/s separation to the simple theory in eq 4 is shown in Figure 13. The parameters used are $\Delta\rho = 45$ kg/m³, $\eta = 0.0025$ Pa \cdot s, and $r = 4$ nm; the other parameters such as the applied acceleration come from the experimental parameters. The expected functionality given by eq 4 is seen in the more resolved 1257 rad/s separation, although the theoretical curve is shifted in position toward further traveled distance. The most likely causes for this disagreement are the simplicity of the model used, rather than the full Lamm equation, and any additional friction due to the downward motion of the iodixanol in response to the applied centripetal acceleration. Motion has been modeled using the Lamm equation by both Arnold et al.⁶ and Nair et al.¹⁴ in predicting the final position of SWCNTs during isopycnic (chirality) separation using ultracentrifugation, and, in both literature results, the redistribution

(29) Bauer, B. J.; Fagan, J. A.; Hobbie, E. K.; Chun, J.; Bajpai, V. J. *Phys. Chem. C* **2008**, *112*, 1842–1850.

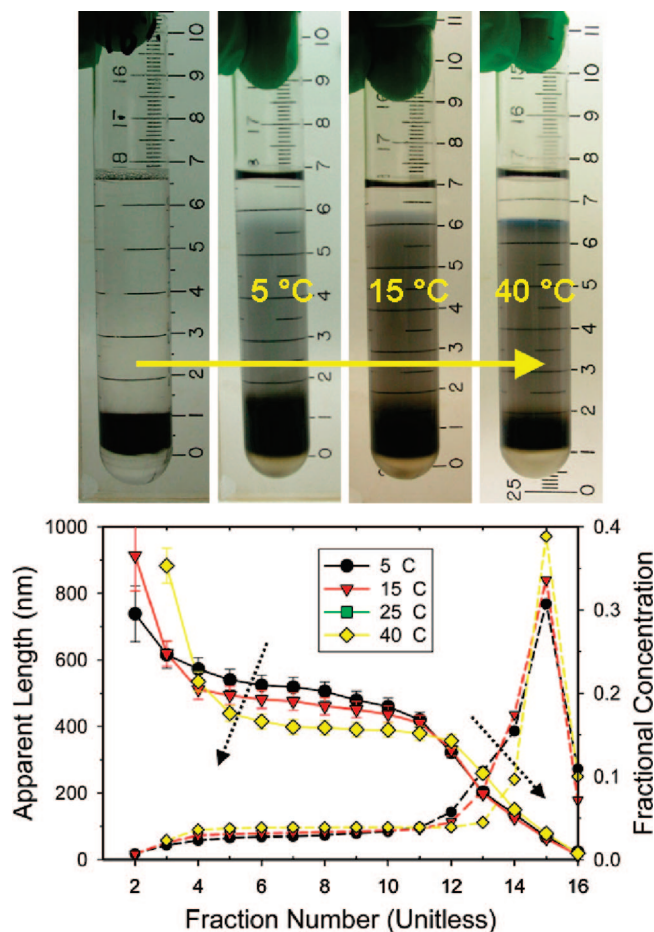


Figure 11. Photographs (top) and apparent SWCNT length versus distance traveled curves (bottom) showing the effect of temperature on the measured length separation performed at 3142 rad/s. Performing the separation at lower temperatures improves the resolution of the fractions, as indicated by the increased slope of the apparent length values. The dashed curves display the fractional concentration, as measured by absorbance at 775 nm, for the displayed separations. The integrated concentration is the same in each experiment. The dotted arrows accentuate the direction of the change with increasing temperature.

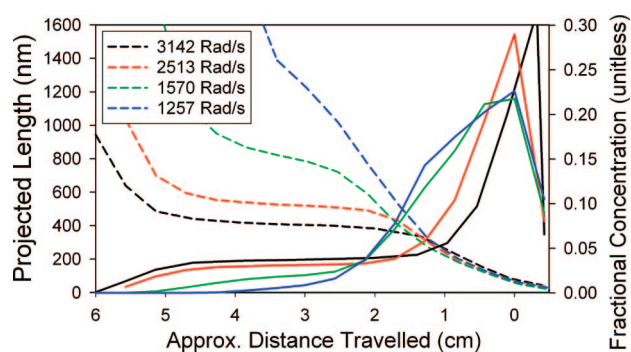


Figure 12. Concentration profiles (solid lines) from the absorbance at 775 nm versus the distance traveled for selected separations shown in Figure 7, and the UV-vis-NIR projected length values from the same separations. The slower separations yield fractions of smaller width as evidenced by the change in the concentration curves while remembering that the injected dispersion was identical in all four experiments. Integration of the curves to calculate the initial average length yields a common value 225 ± 5 nm for all of the curves.

of the iodixanol is significant with centrifugation. We measure, shown in the Supporting Information, that the uppermost two to four fractions are significantly depleted (up to 70% for the top fraction), and the bottommost fractions, numbers 14, 15 and 16,

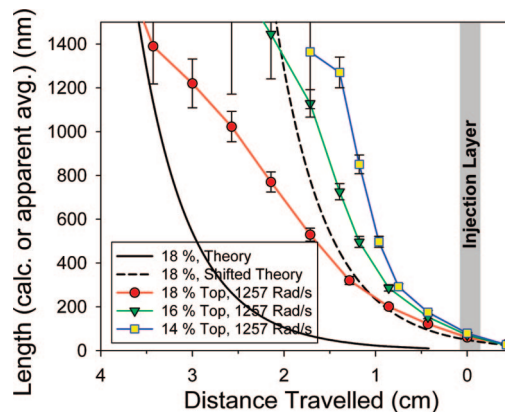


Figure 13. Comparison of the measured average length in each fraction for the 1257 rad/s separation shown in Figure 1 and Figure 2 with the theoretical prediction of eq 4 for an 18% iodixanol top layer. Assuming only eq 4, the theory qualitatively predicts the shape of the separation, but does not quantitatively predict the actual positions of the separated SWCNTs in the experiment. However, eq 4 assumes that the reference frame for the motion of the SWCNTs is the centrifuge tube; however, the density medium is also pelleted during centrifugation, and any additional downward drag from the pelleting iodixanol would, to first order, shift the separation curve to less distance traveled. A uniformly shifted curve approximates the experimental data for a SWCNT-surfactant shell diameter of 8 nm.

increase significantly in iodixanol concentration, during centrifugation. The effect of additional drag would be the measurement of less motion in the static reference frame than is experienced by the traveling object. Empirically shifting the theoretical curve demonstrates that the shape of the measured average length values is consistent with the theory. However, as the amount of additional drag is unknown, a range of r values, $3.2 \text{ nm} < r < 4 \text{ nm}$, yield theoretical curves that approximate the measured data given different empirical shifts.

There are two sets of possible explanations for the observed behavior of the SWCNTs with the separation rate: theories based on SWCNT initiated effects, and theories based on environment initiated effects. Examples of environment-initiated effects would include generation of a sedimentation potential due to the centrifugation rate-dependent rearrangement of the surfactant and iodixanol molecules, driven changes in the surfactant micelle structure due to the intensity of the induced pressure gradient, or generation of convection due to vibrations. SWCNT-initiated effects could include concentration dependent association or aggregation, or alignment effects due to the gradient in centrifugal acceleration. The experiments detailed above allow us to eliminate some of these possibilities.

Given the experimental results, it appears unlikely that external influences from the centrifuge are the cause of the mixing phenomenon. Identical separation at 3142 rad/s is observed using either the (1.59 or 2.54) cm diameter centrifuge tubes, which indicates that vibrations or large flows are not likely causes of the observed behavior. Band broadening effects, sometimes seen in other centrifugation-based separations, and which are caused by an instability that develops when the local density within a fluid element is raised/lowered relative to the surrounding media by the presence of particles (in this case high SWCNT concentration), are also unlikely, as presumably the diameter of the tube would significantly affect this sort of effect. Furthermore, the induction of an apparently similar mixing effect to that observed with an increase in separation rate by increasing the density of the layers at 1257 rad/s implicates the effect as intrinsic to the separation parameters and not solely externally generated. Likewise, the lack of change with the addition of 20 mmol/L

NaCl indicates that charge effects are unlikely to be the cause of the mixing behavior.

Two other types of observations can be extracted from the shown experiments, that there is variation of the separation with the absolute force applied to the individual SWCNTs, and that this behavior is modified by the temperature at which the separation is performed. One possibility that was proposed to account for both phenomena was a temperature dependence to the interactions between the DOC, iodixanol, and the SWCNTs leading to association of SWCNT containing micelle structures in solution at higher temperatures. Association of micelle-wrapped SWCNTs would not likely effect the spectroscopy of the SWCNTs, because of the several nanometer apparent micelle size deduced from the theoretical fit to the separation data in Figure 13, but either alignment of the associate, or carrying of the smaller partner upward could conceivably generate the size mixing phenomena measured with the increased rate of separation and increased solution density. Alignment of an associated SWCNT pair would also be dependent on the absolute intensity of the applied centripetal acceleration; the torque on the associated structure, due to either an uneven hydrodynamic drag on the associate, or from the gradient in centripetal acceleration, would have to be larger than approximately $10 k_B T$ to induce significant alignment. However, both mechanisms are demonstrably too small to account for the experimental results. Under any of the circumstances experimentally accessible in this work, the direct torque due to the gradient in the centripetal acceleration is more than 4 orders of magnitude smaller than $k_B T$; calculation of the torque for the ideal system of a $1 \mu\text{m}$ SWCNT unevenly associated with a 500 nm SWCNT yields that the maximal torque applied in any of the experiments would have been less than $0.2 k_B T$. Neither mechanism would result in significant alignment. These mechanisms are furthermore disfavored, as the formation of associates would be expected to be strongly concentration dependent in a manner increasing with additional SWCNT concentration, opposite to the behavior observed in Figure 9.

Although alignment of a directly associated SWCNT group due to torque cannot account for the experimental results, a separate possibility is that a changing balance of interactions between the SWCNTs, DOC, and iodixanol with temperature and induced pressure drives the formation of structures larger than a single SWCNT, which could affect the separation as experimentally observed. Evidence points toward the generation of larger micelles or condensed surfactant fibrils that extend beyond the SWCNTs due to the high centrifugation induced pressure; either effect would likely lower the effective density of the SWCNTs in the dispersion. For instance, fibrils on the order of millimeters in length are observed if the solutions in which like fractions are being concentrated are run for several days at high speeds. These are likely deoxycholate structures, as the surfactant is known to form fibrils under certain conditions.³⁰ However, it is also likely that the iodixanol is involved. Wei et. al¹¹ report that when using two-component surfactant mixtures to preferentially disperse specific chiralities of small diameter SWCNTs, the presence of 10% iodixanol in the dispersing solution significantly improves the degree of separation, and that the improved separation is not due to a subtle alteration of the buoyancy force on dispersed SWCNTs, but is due to selective individual dispersion of different SWCNT chiralities. Their finding of improved separation in the presence of iodixanol indicates that the iodixanol molecule specifically affects the interactions between SWCNTs and their surfactant solutions.

As the NaChol surfactant used by Wei et. al is closely related to the DOC surfactant used in this work, it is likely that specific effects due to iodixanol may be present in this centrifugation work as well.

In the surfactant condensation theory, the larger structures generated by the applied pressure would template from the ends of the SWCNT micelles, and could either link together disparate SWCNTs, or would otherwise encourage associated motion of the SWCNTs upward to generate the plateau features seen in Figure 8. This theory additionally matches the experimental evidence in that the formation of larger surfactant structures around the SWCNTs would decrease their apparent density, thus resulting in the higher velocities of the longer fractions measured at the higher separation rates. The reduced mixing and plateau features with increased SWCNT concentration could then be consistent with being due to a reduced excess of deoxycholate in solution (per SWCNT) for formation of the fibril, or larger micelle structures.

Although no observation of a structural phase formation or micelle expansion is directly possible in our current experiment, the surfactant condensation hypothesis appears to potentially account for the deviations from the first-order theory observed in the separation experiments. Using the experimental observations, significant optimization is achieved by performing separations at lower temperatures, higher SWCNT concentrations, and low as feasible layer densities. Efforts are underway to verify this surfactant condensation hypothesis.

Lastly, some thought is worthwhile into the economic value of the centrifugation process. An estimate for the cost per milligram of the separation process for the centrifugation techniques on the demonstrated benchtop scale is, for a 1257 rad/s, 96 h separation, assuming no recovery of the density medium, approximately \$6/mg of SWCNTs separated. The cost is primarily associated with the differential rotor cost of approximately \$17000/730 separations per rotor, approximately \$23 per separation, and for the density gradient medium, approximately \$23.50 per separation, to generate 6–10 mg of separated SWCNTs. The SWCNT cost, approximately \$1/mg after dispersion and centrifugation to remove amorphous impurities, the cost of the surfactant, approximately \$1.50 per separation, and the cost of electricity are relatively marginal factors. Recovery of the density medium and shorter separation times, which would allow for up to 2400 runs in the estimated 8 year rotor life span, would dramatically reduce the projected marginal cost. Optimization, utilizing the results of this contribution, allows for separations similar to the 1257 rad/s results to be achieved in 21 h at 2650 rad/s by operating at a lower temperature, 4 °C, and with a less dense top layer. For SEC, in contrast, the current necessity of using custom-made small number oligomer single-stranded DNA to achieve an acceptably robust dispersion introduces an approximate cost of \$15 to \$20/mg of dispersed SWCNTs, prior to even the length separation, solely due to the DNA.

Conclusions

Centrifugation can be used to separate SWCNTs by length. Separation improved with a reduced rate of separation, lower temperature, and higher SWCNT concentration. Lengths for separated fractions measured using AFM, DLS, and UV–vis–NIR extrapolation were found to be in consistent agreement. Longer SWCNTs are found to have stronger optical transitions, consistent with previous results; these long SWCNT display excellent optical properties. Length separation by this method is relatively facile compared to previous techniques, and is

estimated at bench scale to cost less than \$6/mg of separated SWCNTs given recovery of the density inducing iodixanol. Optimizations of the separation, verification of the fibril theory, refinement of the separated SWCNT population through additional processing, and further measurements on the separated fractions are ongoing.

Acknowledgment. The authors gratefully acknowledge support of author Nie through the NIST summer undergraduate research program (SURF). We also thank Southwestern Nanotechnologies, Inc., NASA-JSC, and NanoPower Research

Laboratories for donations of several of the SWCNT soots used as starting materials in this work.

Supporting Information Available: More detailed discussion of the optical length projection, Raman measurements, demonstration of individual dispersion by small angle neutron scattering, and further information on the DLS results. This material is available free of charge via the Internet at <http://pubs.acs.org>.

LA801388A

(30) Marques, E. F.; Edlund, H.; La Mesa, C.; Khan, A. *Langmuir* **2000**, *16*, 5178–5186.